Influence of flame-holder temperature on the acoustic flame transfer functions of a laminar flame

Daniel Mejia, Maxence Brebion, Abdulla Ghani, Thomas Kaiser, Florent Duchaine, Laurent Selle, Thierry Poinsot

▶ **To cite this version:**

Daniel Mejia, Maxence Brebion, Abdulla Ghani, Thomas Kaiser, Florent Duchaine, et al.. Influence of flame-holder temperature on the acoustic flame transfer functions of a laminar flame. Combustion and Flame, 2018, 188, pp.5-12. 10.1016/j.combustflame.2017.09.016 . hal-01730352

HAL Id: hal-01730352
https://hal.science/hal-01730352

Submitted on 13 Mar 2018

HAL is a multi-disciplinary open access archive for the deposit and dissemination of scientific research documents, whether they are published or not. The documents may come from teaching and research institutions in France or abroad, or from public or private research centers.

L'archive ouverte pluridisciplinaire **HAL**, est destinée au dépôt et à la diffusion de documents scientifiques de niveau recherche, publiés ou non, émanant des établissements d'enseignement et de recherche français ou étrangers, des laboratoires publics ou privés.

Open Archive TOULOUSE Archive Ouverte (OATAO)
OATAO is an open access repository that collects the work of Toulouse researchers and makes it freely available over the web where possible.

This is an author-deposited version published in : http://oatao.univ-toulouse.fr/
Eprints ID : 19677

To link to this article : DOI:10.1016/j.combustflame.2017.09.016
URL : http://dx.doi.org/10.1016/j.combustflame.2017.09.016

To cite this version : Mejia, Daniel and Brebion, Maxence and Ghani, Abdulla and Kaiser, Thomas and Duchaine, Florent and Selle, Laurent and Poinsot, Thierry *Influence of flame-holder temperature on the acoustic flame transfer functions of a laminar flame*. (2018) Combustion and Flame, vol. 188. pp. 5-12. ISSN 0010-2180

Any correspondence concerning this service should be sent to the repository administrator: staff-oatao@listes-diff.inp-toulouse.fr

Influence of flame-holder temperature on the acoustic flame transfer functions of a laminar flame

Daniel Mejia[a], Maxence Miguel-Brebion[a], Abdulla Ghani[a], Thomas Kaiser[a], Florent Duchaine[b], Laurent Selle[a,*], Thierry Poinsot[a,b]

[a] *Institut de Mécanique des Fluides de Toulouse (IMFT), Université de Toulouse, CNRS, INPT, UPS, Toulouse, France*
[b] *CERFACS, CFD team, 42 avenue G. Coriolis, Toulouse, France*

A B S T R A C T

The occurrence of combustion instabilities in high-performance engines such as gas turbines is often affected by the thermal state of the engine. For example, strong bursts of pressure fluctuations may occur at cold start for operating conditions that are stable once the engine reaches thermal equilibrium. This observation raises the question of the influence of material temperature on the response of flames to acoustic perturbations. In this study, we assess the influence of the temperature of the flame holder for a laminar flame. Both experiments and numerical simulations show that the Flame Transfer Function (FTF) is strongly affected by the flame-holder temperature. The key factors driving the evolution of the FTF are the flame-root location as well as the modification of the flow, which affects its stability. In the case of the cooled flame-holder, the formation of a recirculation zone is identified as the main impact on the FTF.

Keywords:
DNS
Conjugate heat transfer
Analytically reduced chemistry
Flame transfer function
Premixed flame
Laminar flame

1. Introduction

Experimentalists are aware that the wall temperatures of a combustion chamber affect the thermoacoustic combustion instabilities which can develop in the combustor [1–4]: a chamber does not exhibit the same noise and unstable modes when it starts (and walls are cold) or when it has run for a few minutes (and walls have reached a higher steady temperature). From the modeling point of view, however, most models assume adiabatic flames and do not include any interaction between walls and flames. This is clearly a weak aspect of most Large Eddy Simulation (LES) approaches for turbulent burners. Among all the walls found in a combustion chamber, flameholders play a very specific role: this is where flames are anchored and where they are the most sensitive to heat transfer. Any temperature change of the solid in the region where flames are stabilized can change not only its stabilization point (the place where it is anchored) but also its dynamics (its response to acoustic waves as well as its blow-off limits). The MIT group used DNS to study the stabilization of premixed flames on square flame holders [5–7] and showed that the location of the flame roots and the blow-off limits were strongly affected by the temperature of the flameholder. Kaess et al. [8] proved that the temperature of a laminar flame stabilized in a dump combustor controlled the flame response to acoustic waves. Duchaine et al. [9] used sensitivity analysis on a DNS to show that the acoustic response of flames stabilized by a backward facing step depended strongly on the wall temperatures. Mejia et al. [3] demonstrated experimentally that controlling the wall temperature of a 2D triangular laminar flame was sufficient to bring it in and out of thermoacoustic oscillations. These conclusions, obtained for laminar flames, have been confirmed for turbulent flames [10,11]. [10] showed that the thermal conductivity of the backward step blocks used to stabilize a turbulent flame, controlled the level of self-sustained instability.

The present work focuses on laminar flames and analyzes the acoustic response of V-flames stabilized on a two-dimensional cylinder which can be water cooled to fully control its temperature between 300 and 700 K. The setup corresponds to the one used by Miguel-Brebion et al. [12]: a laminar methane/air flame is stabilized on a cylinder where the temperature of this cylinder is controlled by water cooling. Miguel-Brebion et al. [12] described the different flame topologies and stabilization positions observed when the flame-holder temperature was changed. When it comes to describing the capacity of these flames to create self-excited instability modes, the most useful quantity to consider is the Flame Transfer Function (FTF) $\mathcal{F}(\omega)$ which measures the normalized variations of the global reaction rate $(q'/\bar{q})$ induced by a normalized inlet acoustic velocity pulsation (u'/u_b) [2,13,14]:

$$\mathcal{F}(\omega) = \frac{q'/\bar{q}}{u'/u_b}$$

* Corresponding author.
E-mail addresses: laurent.selle@imft.fr, selle@imft.fr (L. Selle).

https://doi.org/10.1016/j.combustflame.2017.09.016

FTF's can be obtained experimentally or numerically: both methods will be used here. The present study focuses on measurements of FTF in the setup of Miguel-Brebion et al. [12] and shows that the FTF are extremely sensitive to the flameholder temperature which appears to be a first-order parameter controlling the FTF in terms of gain and phase. One of the new results obtained here is that this effects of the flame holder temperature is due not only to a modification of the flame root dynamics, close to the flame holder but also to a drastic change of the mean flow itself, far downstream as seen in [15], but in this case induced by the creation of a large recirculation zone when the flame holder is cooled.

The paper combines experimental measurements and direct numerical simulation (DNS) results to analyze the FTF's of a lean premixed laminar methane/air flame. Simulations are performed in dual mode: the flow is computed with DNS using a 19 species kinetic scheme for CH_4/air flames [16] while the temperature in the solid is computed with a heat transfer solver, coupled to the flow solver. The experiment uses a multi-microphone technique and hot wire measurements to quantify u' as well as unsteady CH^* chemiluminescence and high speed imaginary to evaluate $\dot{q}'$.

The paper is organized as follows: the configuration is briefly described in Section 2. The experimental set-up used to measure the FTF's is described in Section 3. The DNS tools used to compute the FTF of the flames are described in Section 4. Finally a discussion of the results obtained experimentally and numerically is presented in Section 5.

2. Configuration

The experimental bench consist of a lean premixed methane–air V-flame stabilized in the wake of a steel cylindrical bluff body (diameter $d = 8$ mm). The burner has a constant cross section of $h = 34$ mm by $l = 94$ mm so that the flame remains two-dimensional, allowing faster DNS (Section 4). The Reynolds number based on the bluff-body diameter $Re_{cyl} \approx 500$ is low enough to ensure laminar flow. The reactants are premixed in a one-meter long injection tube and equally distributed to six injectors placed at the bottom of the injection chamber. The flow is laminarized by an array of small glass balls and one honeycomb panel and passes through the cooled plenum to ensure a constant fresh-gases temperature. Finally, it enters the combustion chamber where the bluff-body is located. The lateral sides of the combustion chamber are water cooled to impose the wall temperature. The plenum has three pressure plugs and one loudspeaker plug at each side. The combustion chamber has three optical accesses: one at the front to allow a direct view of the flame and one 3 mm slot on each for the laser sheet.

Two different bluff-bodies are used to stabilize the flame. The first, called CBB (Cooled Bluff-Body), is a steel water-cooled cylinder (Fig. 2, left). Drilled holes at the end of the feeding line allow the water to flow to the 6 mm outer line, where it is evacuated. The cooling system is designed to maintain temperatures around 285 K in the bluff-body walls. The second flame holder, called UBB (Uncooled Bluff-Body) is a full, solid, steel cylinder, with the same external diameter as the cooled one (Fig. 2, right). Its temperature is not controlled and depends on the flame shape. It can reach up to 700 K.

The operating condition is the same for all cases (Table 1). For this regime and this geometry of the chamber, there is no combustion instabilities (CI) so that the flame is steady. The burner power is 7 kW for an equivalence ratio $\Phi = 0.75$ and a bulk velocity $u_b = 1.07$ ms^{-1}. The flame holder temperature is measured with a K-type thermocouple: $T_{cyl}^{\mathrm{UBB}} = 670 \pm 40$ K. In the CBB case, the temperature elevation of the water used for cooling is equal to $\Delta T = 0.15 \pm 0.05$ K so that the cooling water temperature can be assumed to be constant. The total flux taken from the flame is

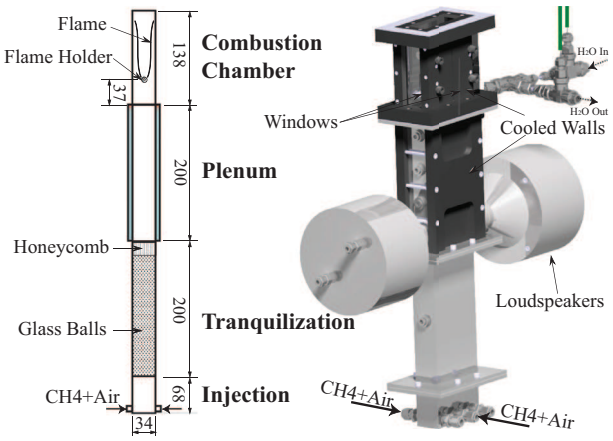

Fig. 1. Transverse cut (*left*) and isometric view (*right*) of the Intrig burner.

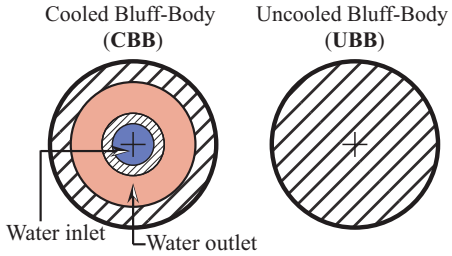

Fig. 2. Cooled bluff-body, CBB $T_w \approx 285$ K (*left*) and uncooled bluff-body, UBB $T_w \approx 700$ K (*right*).

Table 1
Operating conditions.

Name	Quantity	Value
Φ	Equivalence ratio	0.75
u_b	Bulk velocity	1.07 ms^{-1}
s_l	Laminar flame speed	0.24 ms^{-1}
T_u	Injection temperature	292 K
T_{adia}	Adiabatic flame temperature	1920 K

Table 2
Thermal properties of the flame-holder steel. The emissivity ϵ ranges from 0.2 for polished surfaces to 0.9 for oxidized surfaces.

Material	ρc_p [K^{-1}m^{-3}]	λ [W/m/K]	ϵ
35NCD16	$3.5\,10^6$	32	0.9

$\Phi_{s\to w}^{\mathrm{xp}} = \dot{m} C p \Delta T = 24$ W. The thermal properties of the steel used in both UBB and CBB cases are given in Table 2. In this configuration, Miguel-Brebion et al.. have shown that radiation form the flame holder is a key factor to predict the temperature of the UBB case. In the present experiments, bluff-bodies are oxidized so that an emissivity of $\epsilon = 0.9$ is retained.

3. Experimental strategy

The determination of the FTF (*cf.* Eq. 2) requires the knowledge of the heat release rate fluctuations. For a perfectly premixed mixture at a given equivalence ratio, the heat release rate $\dot{q}$ is proportional to the flame surface, $\mathcal{A}$, and to the light emission, I, from free radicals CH^* [17–19], and it is possible to determine the transfer function from one of the following expressions:

$$\mathcal{F}(\omega) = \frac{\dot{q}'(t)/\bar{\dot{q}}}{u'(t)/u_b} = \frac{\mathcal{A}'(t)/\bar{\mathcal{A}}}{u'(t)/u_b} = \frac{I'(t)/\bar{I}}{u'(t)/u_b}$$

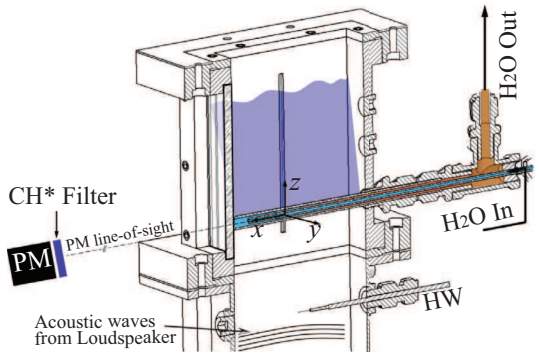

Fig. 3. Iso-transverse cut of the experimental configuration used to measure the FTF (CBB configuration).

To reduce the error due to experimental noise the flame transfer function may be calculated by:

$$\mathcal{F}(\omega) = \frac{\mathcal{S}_{uq}(\omega)}{\mathcal{S}_{uu}(\omega)} \tag{3}$$

Where, $\mathcal{S}_{uq}$ is the cross power spectral density between the $u'(t)/u_b$ and $I'(t)/\bar{I}$ signals and $\mathcal{S}_{uu}$ is the power spectral density of the velocity signal, $u'(t)/u_b$. The flame is excited with a pure sinusoidal acoustic signal, and the Fourier transform of the input and output signal is calculated at exactly the forcing frequency. The gain is defined as the magnitude of $\mathcal{F}(\omega)$, $\mathcal{G} = |\mathcal{F}(\omega)|$ while the phase is its argument, $\varphi = \arg[\mathcal{F}(\omega)]$.

3.1. Experimental measurements

Measuring the complex number $\mathcal{F}(\omega)$, requires a stable configuration that can be pulsated over the range of frequencies where the flame is sensitive to acoustic perturbations. Two loudspeakers placed at the bottom of the plenum are used to send phased planar harmonic acoustic waves towards the flame. Light emission from CH* free radicals, I' and velocity fluctuations u' are recorded simultaneously by the photomultiplier (PM) and the hot-wire probe (HW) represented in Fig. 3, respectively. The HW is placed at the center of the plenum through a pressure plug located at $(x, y, z) = (0, 0, -61$ mm$)$ and it is oriented to measure the velocity component u_z. The PM axis is aligned with the cylinder centreline axis (x) and it collects the 2D line-of sight integrated flame CH* light emission.

Durox et al. [20] showed that for these flames, the gain of the FTF strongly depends on the amplitude of the velocity fluctuations, even for low amplitudes (5–10% of the bulk velocity). In order to avoid non linear-effects, the amplitude of the velocity perturbation is kept as low as possible, while preserving a good signal to noise ratio (SNR). Without modulation, the rms velocity fluctuations are less than 0.4% of the bulk velocity: a velocity modulation amplitude of 1% of the bulk velocity is enough to have at least a SNR of 2. Figure 4 is an example of the time traces, over three acoustic periods, of the normalized velocity and heat release rate, for an excitation frequency of $f_{ex} = 100$ Hz and an amplitude of $u'/u_b = 0.01$.

The FTF corresponds to the mean value of four runs at each frequency. The gain and the phase of the FTF for the two cases CBB and UBB are presented in Fig. 5. In both cases the gain $\mathcal{G}(\omega)$ starts from unity at low frequencies, reaches a maximum around $f_{ex} =$ 100 Hz and returns to zero at high frequencies above $f_{ex} > 250$ Hz. The amplitude of the peaks, however, varies considerably from one case to another. In UBB case, the peak amplitude is close to $\mathcal{G} \approx$ 2.5 while for the cooled case CBB it reaches values close to 4.0.

Phases $(\varphi = \arg[\mathcal{F}(\omega)])$ increase linearly for both cases. However, the slope of $\varphi(\omega)$, which corresponds to the time delay

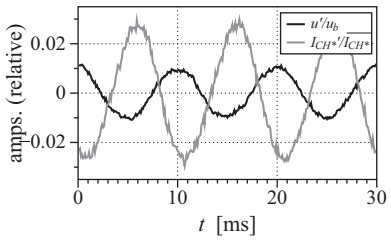

Fig. 4. Experimental results: time traces of normalized velocity (——) and heat release rate (——) for a frequency of $f_{ex} = 100$ Hz and a modulation amplitude of $u'/u = 0.01$ in the UBB configuration.

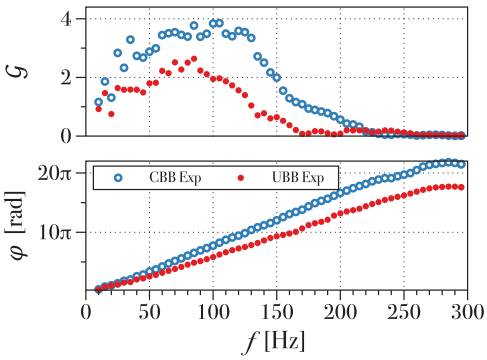

Fig. 5. Experimental results: gain (*top*) and phase (*bottom*) of the FTF for both CBB (○) and UBB (●) cases, for excitation frequency of $f_{ex} = 100$ Hz and an amplitude of $u'/u_b = 0.01$.

$(\tau = \varphi/\omega)$ between the acoustic perturbation and the heat release rate response, is different. The time delay τ decreases with the flame holder temperature, it goes from 45 ms in the CBB case to 35 ms for the UBB case.

Figure 5 brings up two important results:

- The change of temperature of the flame holder has a major effect on both gain and phase of the FTF.
- The absolute values of gain are very large for these flames (from 2.5 to 4). Such values have already been reported for conical "V" flames [20,21]. They are due to the 2D nature of the flames and are analyzed in the next section where the DNS of the same flames are performed.

4. Numerical strategy

To capture the effects of flame holder cooling on the FTF, a coupled DNS of the flow and of the temperature field within the flame holder is performed. The choice of a 2D configuration allows the use of high order schemes and complex chemistry to properly describe the near wall chemistry.

4.1. Fluid and solid solver

The compressible Navier Stokes equations are solved with the AVBP solver using a third-order scheme for spatial differencing on a two-dimensional hybrid mesh combined with an explicit two-step scheme for time advancement [22,23]. The NSCBC formulation [2,24] is used for the boundaries while the molecular transport description is based on the Hirshfelder Curtis approximation [25]. A multistep analytical mechanism, referred to as LU19 is used to describe the chemical kinetics of the methane–air combustion [16].[1]

[1] This chemical mechanism was used instead of the 13-species schemes used in Miguel-Brebion et al. [12] because it provides better results for the flame position [26]: this is consistent with the fact that it takes into account more species and

The resolution of the heat transfer equation in the bluff-body relies on an implicit [27] first-order forward Euler scheme for time integration and a second-order Galerkin scheme [28]. Local heat fluxes ϕ_s are imposed in the solid solver at the boundary shared between the solid and the fluid domains. The solid solver then sends skin temperatures back to the DNS code for the next iteration.

4.2. Coupling strategy

The DNS code (around the cylinder) and the heat transfer solver (in the cylinder) are coupled with a software called OpenPALM [29] which exchanges heat fluxes and temperatures on the cylinder skin. The local temperature obtained by the solid solver on the cylinder surface solver is applied through an isothermal NSCBC boundary condition [24] in AVBP whereas the local heat flux is given by AVBP to solid solver. The characteristic flow time τ_f is of the order of 50 ms while the solid characteristic time τ_s is of the order of 100 s. The simulation of the flame for several τ_s is impractical but it is not needed since the bluff-body temperature changes very slowly and only the steady-state temperature field is relevant here. Therefore, the coupling strategy to accelerate the convergence towards steady state is that each domain (flow and solid) is advanced at its own characteristic time using a time step $\alpha_f\ \tau_f$ for the fluid and $\alpha_s\ \tau_s$ for the solid with $\alpha_f = \alpha_s$ [9]. This is sufficient to obtain steady state values of the cylinder temperature. This temperature is almost constant when flames are acoustically forced so that only the flow solver is running when computing the FTF's.

Moreover, radiative heat losses from the flame holder must be accounted for when relatively high temperatures are reached. They are taken into account in the local flux condition imposed on in the solid solver by adding a radiative flux ϕ_{rad}:

$$\phi_{rad} = \sigma\epsilon(T^4 - T_{ext}^4) \tag{4}$$

where σ is the Boltzmann constant, ϵ is the emissivity coefficient of the bluff-body surface and T is its local temperature. Radiation from the gas (H_2O, CO_2) and from the hot walls downstream of the combustion zone is neglected. Furthermore, walls at the same height of the flame holder are assumed to have a temperature close to the fresh gas and to behave as black bodies: $T_{ext} = T_u = 300$ K. This simple coupling strategy has been already used in several studies with good results [12,30].

4.3. Simulated domain and mesh

The computation of realistic flame dynamics responses must take into account the interaction between the flame and the external walls. Thus, the whole flame must be calculated. The simulated domain used to calculate FTFs has been specifically adapted: the plenum has been kept as short as possible while the chamber was kept identical to the experimental one (Fig. 6). The mean velocity profile has been measured experimentally 35 mm upstream of the cylinder and is imposed at the DNS inlet while the combustion chamber walls are cooled. Cooling the external walls simplifies the set-up of the DNS because a simple isothermal boundary condition is imposed at the DNS side walls.

An unstructured hybrid mesh, [12], is used to accurately capture the conjugate heat transfer between the solid and the reactive flow [31,32]. Five layers of quad elements are used outside of the cylinder boundary (flow region) and ten are used inside (solid region). The remaining parts of the geometries are meshed with triangles (Fig. 6). The meshes for solid and fluid domains are not coincident

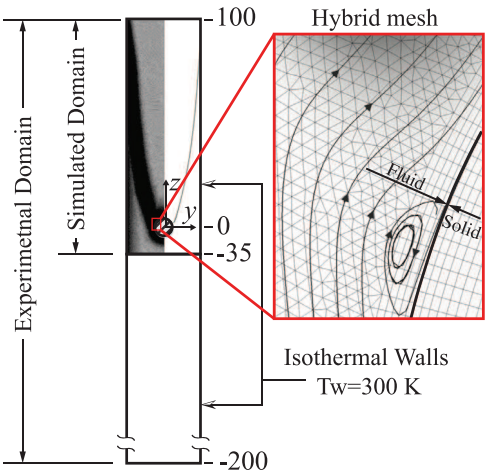

Fig. 6. Comparison between the experiment and computational domain. With a zoom on the mesh. The stream lines show that the recirculation zone is well captured by the hybrid mesh.

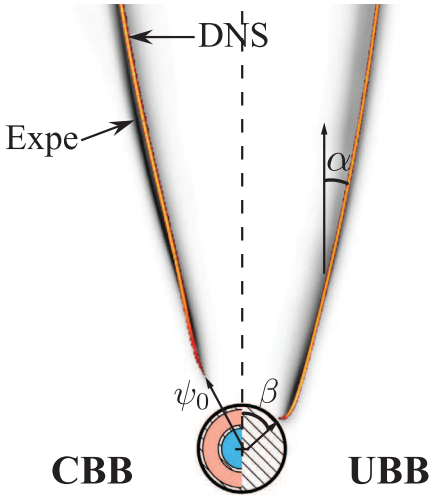

Fig. 7. Comparison between the experimental and simulated flames for the CBB and UBB cases.

on the flame holder skin and a second-order in space interpolation is performed to transfer information between the two solvers. The mesh is refined along the flame front and close to the bluff-body. A convergence study was performed in a stationary flame [12] and a mesh resolution of 70 μm is retained providing at least 8 cells in the flame region.

In order to validate the choices made above a comparison between the experimental and the simulated stationary flame is shown in Fig. 7, for the CBB and UBB cases. The experimental flame corresponds to a line of sight integrated CH^* field.

In both cases, the flame shape and the flame anchoring position are well reproduced by the DNS. To first order, the FTF is controlled by the stationary flame shape [33,34], determined by the flame angle α (Table 7), for long flames $\alpha \approx \tan^{-1} s_{l_0}/u_b$. A good agreement is found between experiments and DNS (Table 3). Another important aspect controlling the FTF is the flame anchoring mechanism. The flame stand-off distance, ψ_0, is defined as the distance between the flame holder and the flame root (Fig. 7). Recent studies have shown that small changes ψ_0 can have significant impact on the flame dynamics [3,14,35,36]. Figure 7 and Table 3 show good agreement for ψ_0 between experiments and DNS.

reactions and predicts a more precise flame velocity. The 19-species scheme also provides a better description of low-temperature chemistry near the cylinder.

Table 3
Comparison between the flame stationary parameters of the flame shape for CBB and UBB cases. ψ_0 is the flame stand off distance and α is the flame angle.

Parameters	CBB		UBB	
	Exp.	DNS	Exp.	DNS
α [rad]	0.09π	0.07π	0.08π	0.07π
ψ_0 [1/D]	0.95	0.94	0.64	0.52

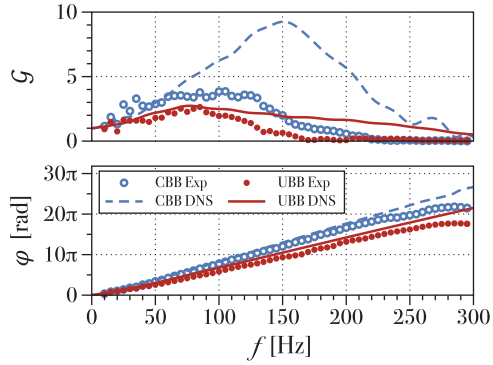

Fig. 8. Flame Transfer Function (FTF) for the two configurations in DNS CBB (– – –) and UBB (▬▬) along with the previous experimental results CBB (○) and UBB (●).

This steady-state analysis allows to conclude that the essential parameters, α and ψ_0, controlling the FTF, are well reproduced by the DNS. Therefore we can proceed to calculate the numerical FTF.

4.4. Flame transfer function calculation

There are two main methods to measure Flame transfer functions for a linear invariant system. [37–40]:

- Forcing with a single frequency to obtain both FTF [41,42] or FDF [39,43–45].
- Forcing with a broadband signal and using Wiener-Hopf system inversion [40,46–48] to retrieve the FTF.

Harmonic forcing can be CPU intensive since one simulation per frequency is required. Nevertheless, it is possible to pulsate at different amplitudes, allowing to explore the flame response in both linear and non-linear regime. On the other hand, the broadband noise forcing method can be more frugal since one can obtain the FTF for the whole range of frequencies in one run. However, broadband is only suitable in the linear regime when the heat release perturbation remains small. Here, we use the broadband method [48] to obtain the FTF's in the linear regime for the two cases[2].

The FTF was calculated for the CBB and UBB configurations. The amplitude of the velocity fluctuations is kept under 1% of the bulk velocity ($u'/u_b < 0.01$).

The gains and phases of the FTFs from experiments and simulations are presented in Fig. 8 along with the FTF experimental results. The agreement is very good for the phase and confirms the influence of the flame holder temperature seen in the experiments. In the UBB case, the agreement on the gain is also fair, however, past the peak that is around 80 Hz, the gain decreases faster in the experiment than in the DNS. In the CBB case, however, the agreement in the gain is less satisfactory: The value of the maximum gain obtained by the DNS exceeds by a factor of two the one found in the experiments. This discrepancy is due to the fact that, unlike the stationary flame that fits in the visualization window, the pulsated flame sometimes leaves the field of view of the PM. During some part of the acoustic cycle, the flame tip leaves the domain, making impossible for the PM to capture the total heat release rate fluctuation. This is not the case in the UBB case, because, as seen in Fig. 7, the flame is closer to the cylinder and the tip of the flame remains inside the field of view of the PM during the whole acoustic cycle. Globally, experiments and simulations show the same trend and a simple conclusion arises: as the temperature of the bluff-body decreases (UBB → CBB), the gain and the delay of the FTF both increase. The changes of the FTF are large and the maximum gain of $\mathcal{F}(\omega)$ can change by a factor of two (in the simulations) when the bluff-body temperature goes from 300 to 700 K.

5. Discussion

5.1. Flame front fluctuations

We propose to investigate the discrepancy between the FTF gains for the CBB configuration by tracking the instantaneous flame front fluctuations. Here the flame was pulsated at $f_{ex} = 100$ Hz, in both experiments and DNS, and the acoustic velocity amplitude was set to a sufficiently high value ($u'/u_b = 0.05$) for the two cases in order to magnify the flame surface displacement. It is well known that V-shape flames are very sensitive to non linearities, increasing the amplitude of the acoustic perturbation usually decreases the gain of the FTF ([20]). However, for this flame, it was checked that at 100 Hz, the influence of flame-holder cooling is similar at 1% and 5% pulsation amplitude, therefore validating the increase for the flame front study.

In the experiments the flame images were recorded with a 1280 × 800 pixels Phantom V1210 high-speed camera equipped with a 700 nm low-pass infrared filter (to eliminate the burnt gases emission, and increase the contrast) and a Nikkor lens (focal length 200 mm/aperture 4). Li et al. [19] showed that it is not necessary to operate with an interference filter (CH^* or OH^* for example) in front of the camera to examine heat release rate fluctuations of laminar premixed flames from hydrocarbon fuels submitted to flowrate disturbances when the equivalence ratio, Φ, is lower than 1.2. The camera is triggered by the velocity signal, it starts recording at a rate of 5000 fps when the velocity fluctuation at the reference point reaches its first maximum (the amplitude of the velocity fluctuation is fixed to 1% of the bulk velocity). The camera records during 4 s which give us 20,000 images. Then the images are averaged to obtain one image, which is the average of 4000 images, every 1/50 of the period. In the DNS the flame front is tracked as an isocontour of heat release rate set at 20% of the maximum reaction rate in the corresponding freely propagating laminar flame.

Figures 9 and 10 show the experimental and numerical instantaneous flame fronts for four different excitation phases for the CBB and UBB cases, respectively. In both cases, wrinkles are propagated along the flame front at the convective speed u_b. These wrinkles are created in the vicinity of the flame holder, where the flame is attached. The agreement between experiments and simulations is very good for both cases and the amplitude of the wrinkles is well reproduced by the DNS. One can also notice that the flame is anchored closer to the flame holder in the UBB case, which is consistent with the results of [12]. Figures 9 and 10 show that for the same amplitude, the wrinkles are more pronounced in the cooled case. This is coherent with the higher FTF gain for the CBB configuration (Fig. 5).

A proper framework to analyse the wrinkles observed in Fig. 9 and 10 is the G-equation approach [33,49]. Figure 11 is a

[2] The harmonic response method was used, to validate the results of the broadband noise, for a single excitation frequency of $f_{ex} = 100$ Hz and a velocity fluctuation amplitude of $u'/u_b = 0.01$. No difference was found between the two methods.

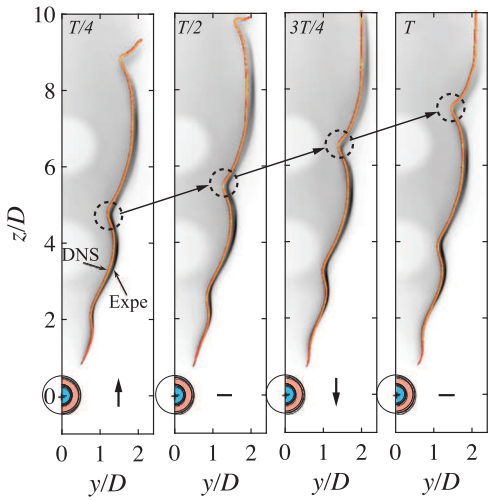

Fig. 9. Experimental and numerical instantaneous flame front during one acoustic period of excitation for the CBB case at a frequency of 100 Hz and an amplitude of 5% of the bulk velocity. The black arrow represents the instantaneous direction of the acoustic velocity fluctuation at the reference velocity location ($z = -61$ and $z = -20$ mm upstream of the cylinder for the experiments and the DNS respectively).

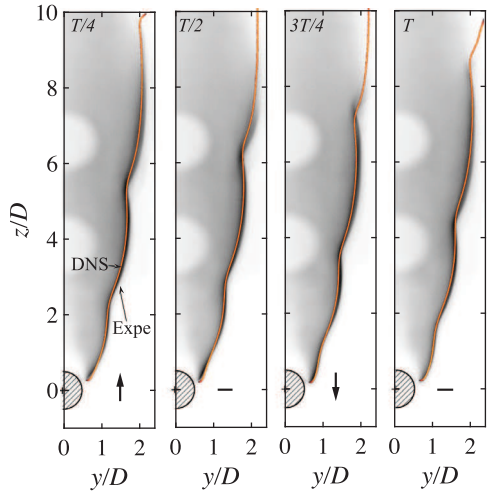

Fig. 10. Experimental and numerical instantaneous flame front during one acoustic period of excitation for the CBB case at a frequency of 100 Hz and an amplitude of 5% of the bulk velocity. The black arrow represents the instantaneous direction of the acoustic velocity fluctuation at the reference velocity location ($z = -61$ and $z = -20$ mm upstream of the cylinder for the experiments and the DNS respectively).

schematic representation of the perturbed flame front with the laboratory (z, y) and the steady flame (Z, Y) reference frames, α corresponds the steady flame angle with respect to the mean flow direction. The instantaneous flame front position relative to the steady flame is given by $\xi(Y, t)$. The amplitude of the flame front fluctuation normal to the steady flame front $\tilde{\xi}_Z$ is shown in Fig. 12 for both cases CBB and UBB. Experiments and DNS provide very consistent results. Figure 12 shows that flame wrinkles are linearly amplified along the flame front as already described in [50]. In the CBB case the growth rate of the amplification is larger than in the UBB case. The flame holder temperature is the only parameter varying in the two different cases and all other parameters such as bulk velocity, equivalence ratio, external wall temperature and fresh gases temperature remain constant.

Additional information can be obtained by looking at the flame root trajectories (Fig. 13). In the UBB case the flame root goes back and forth along a single line, induced by the acoustic forcing. On

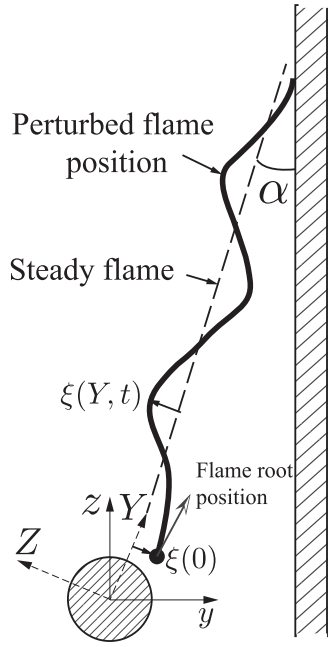

Fig. 11. Schematic representation of the perturbed flame front in the G-equation framework.

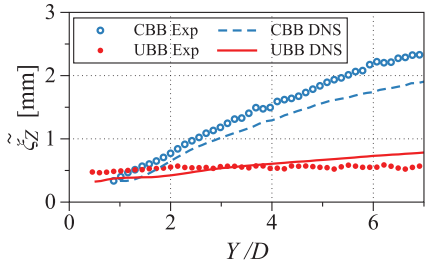

Fig. 12. Experimental and numerical amplitude of the flame front fluctuation normal to the steady flame front $\tilde{\xi}_Z$, for both cases CBB and UBB.

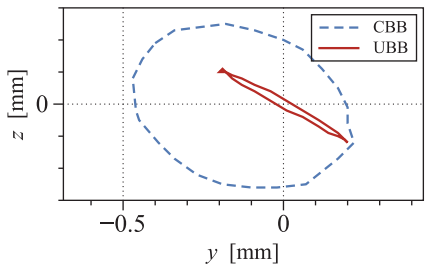

Fig. 13. DNS flame root trajectories in the (y, z) plane for the two configurations CBB (– – –) and UBB (——).

the other hand, the CBB flame root moves in a circular pattern suggesting the presence of a vortex in the stabilization region as discussed in the next section.

5.2. Mean flow field

Figure 12 shows that the growth rate of the flame wrinkles is larger for the CBB than for UBB. This suggests a modification of the mean velocity field downstream the cylinder caused by the flame holder temperature difference between the two cases. Figure 14 shows a comparison between the two mean DNS axial velocity fields for the CBB and UBB flames. Upstream of the cylinder, the mean velocity field is not affected by the cylinder temperature.

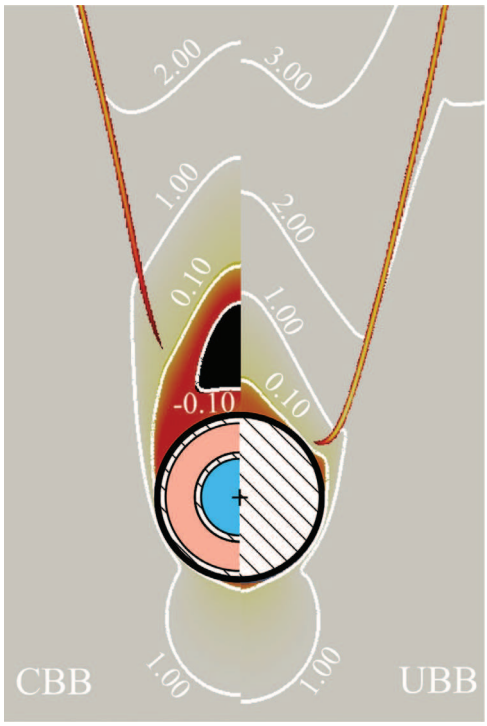

Fig. 14. DNS mean axial velocity fields for CBB and UBB configurations. White lines represent iso-contours of mean axial velocity u.

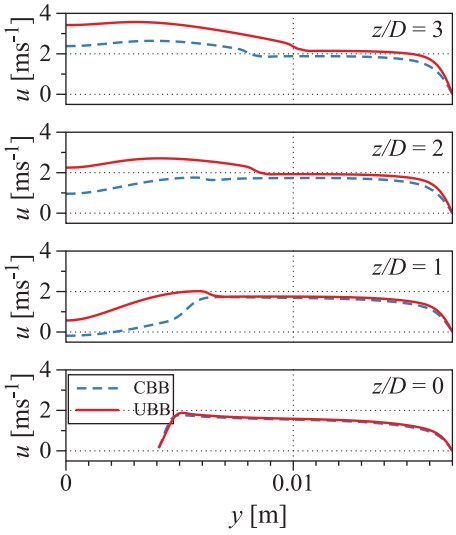

Fig. 15. DNS mean axial velocity profiles for both configurations, CBB (- - -) and UBB (▬) and four different axial positions $z/D = 0$, 1, 2 and 3.

However, downstream of the cylinder, the CBB flow exhibit a large recirculation zone with negative axial velocity (Fig. 14 *left*). This negative velocity zone is not present in the UBB case (Fig. 14 *right*).

This information is confirmed by looking at the mean axial velocity profiles for both configurations and four different axial positions $z/D = 0$, 1, 2 and 3 (Fig. 15). The velocity profiles at the center of the cylinder ($z/D = 0$) are the same for the CBB and UBB case. However, downstream of the cylinder (z/D =1, 2 and 3) the velocity profiles are very different: the CBB case exhibits negative velocities at $z/D = 1$ and still differs from its UBB counterpart far downstream: obviously, this also induces different hydrodynamic stability curves and perturbations which are more amplified for the CBB case. At $z/D = 1$, for example the CBB flow field still exhibits a backflow zone and therefore, a higher hydrodynamic sensibility to perturbations. This may explains why flame perturbations grow faster for the CBB than they do for the UBB case (Fig. 12). This result confirms that the influence of the flame holder temperature is not limited to its immediate vicinity. When the flame holder temperature is brought down from 700 K (case UBB) to 300 K (CBB), it affects the flame response in two ways. First, the flame root position is pushed away from the bluff body (Fig. 7). Even though this effect is the most obvious, it is not the most important one. The second effect is that the whole flow field downstream of the cylinder is changed: a large recirculation zone appears in the CBB case (Fig. 15), leading to a flow which is more hydrodynamically unstable and which amplifies flame front perturbations more strongly as revealed by Fig. 12. This indicates a global effect of the flame holder temperature on the whole flow field and not only a local effect on the flame root location in the vicinity of the bluff body.

6. Conclusion

This paper describes a study of the flame holder temperature influence on the response of laminar premixed flames to acoustic oscillations. Experiments and DNS are used to calculate the FTF's for two different configurations, a cooled flame holder, CBB case, with a temperature of 285 K, and an uncooled flame holder, UBB case with a temperature of 700 K. The experiments and DNS show consistent results: the flame holder temperature has a large impact on the FTF's of these flames, for both gain and phase. The CBB configuration shows a stronger response for the same amplitude of velocity fluctuations. This effect is also seen in the instantaneous flame front fluctuations (Fig. 9). Far downstream of the cylinder the flame wrinkles are much larger for the CBB case than for the UBB case.

The amplitude of the flame wrinkles created in the near wake of the cylinder are of the same order of magnitude for both flames but the growth of these wrinkles is much larger for the CBB case than it is for the UBB case (Fig. 12). This growth is observed far downstream of the cylinder and is due to the fact that the mean velocity fields in the UBB and the CCB cases differ not only close to the cylinder but also far downstream. The flame presence close to the cylinder in the UBB case completely destroys the recirculation zone observed in the CBB case where the flame is stabilized further away from the cylinder (Fig. 15). The velocity profile in the CBB case exhibits negative velocities and still differs from its UBB counterpart far downstream: obviously, this also induces different hydrodynamic stability curves and perturbations which are more amplified for the CBB case. This result confirms that the influence of the flame holder temperature is not limited to its immediate vicinity. It affects both the flame position and the mean velocity field so that the flame wrinkles are affected in two ways: (1) the flame root position is shifted downstream when the flame holder is cold and (2) the mean flow is also changed everywhere downstream: the CBB case exhibits a strong recirculation zone and a stronger growth rate for flame perturbations.

These results demonstrate that the temperature of the flame holder play a major role on the flame position and the mean flow as well as on the flame dynamics where it controls the FTF's to a large extent. Studing flames stabilized on bluff bodies should include their flame holder temperature as a major control parameter.

Acknowledgment

This work was granted access to the high-performance computing resources of CINES under the allocation A0012B07036 made by Grand Equipement National de Calcul Intensif. The research leading to these results has received funding from the European Research Council under the European Union's Seventh

Framework Programme (FP/2007-2013) / ERC Grant Agreement ERC-AdG 319067-INTECOCIS.

References

[1] T. Lieuwen, Nonlinear kinematic response of premixed flames to harmonic velocity disturbances, Proc. Combust. Inst. 30 (2) (2005) 1725–1732.

[2] T. Poinsot, D. Veynante, Theoretical and numerical combustion, 2011. Third Edition (www.cerfacs.fr/elearning)

[3] D. Mejia, L. Selle, R. Bazile, T. Poinsot, Wall-temperature effects on flame response to acoustic oscillations, Proc. Combust. Inst. 35 (3) (2015) 3201–3208.

[4] T. Poinsot, Prediction and control of combustion instabilities in real engines, Proc. Combust. Inst. 36 (1) (2017) 1–28.

[5] K.S. Kedia, C. Safta, J. Ray, H.N. Najm, A.F. Ghoniem, A second-order coupled immersed boundary-SAMR construction for chemically reacting flow over a heat-conducting Cartesian grid-conforming solid, J. Comput. Phys. 272 (2014) 408–428.

[6] K.S. Kedia, A.F. Ghoniem, The anchoring mechanism of a bluff-body stabilized laminar premixed flame, Combust. Flame 161 (9) (2014) 2327–2339.

[7] K.S. Kedia, A.F. Ghoniem, The response of a harmonically forced premixed flame stabilized on a heat-conducting bluff-body, Proc. Combust. Inst. 35 (1) (2015) 1065–1072.

[8] R. Kaess, W. Polifke, T. Poinsot, N. Noiray, D. Durox, T. Schuller, S. Candel, Cfd-based mapping of the thermo-acoustic stability of a laminar premix burner, Summer Program (2008), pp. 289–302.

[9] F. Duchaine, S. Mendez, F. Nicoud, A. Corpron, V. Moureau, T. Poinsot, Conjugate heat transfer with large eddy simulation for gas turbine components, Comptes Rendus Mécanique 7 (6–7) (2009) 550–561.

[10] S. Hong, S. Shanbhogue, K. Kedia, A. Ghoniem, Impact of the flame-holder heat-transfer characteristics on the onset of combustion instability, Combust. Sci. Technol. 185 (2013) 1541–1567.

[11] A. Ghani, M. Miguel-Brebion, L. Selle, F. Duchaine, T. Poinsot, Effect of wall heat transfer on screech in a turbulent premixed combustor, Summer Program (2016), pp. 133–142.

[12] M. Miguel-Brebion, D. Mejia, P. Xavier, F. Duchaine, B. Bedat, L. Selle, T. Poinsot, Joint experimental and numerical study of the influence of flame holder temperature on the stabilization of a laminar methane flame on a cylinder, Combust. Flame 172 (2016) 153–161.

[13] A. Kaufmann, F. Nicoud, T. Poinsot, Flow forcing techniques for numerical simulation of combustion instabilities, Combust. Flame 131 (4) (2002) 371–385.

[14] K. Kedia, H. Altay, A. Ghoniem, Impact of flame–wall interaction on premixed flame dynamics and transfer function characteristics, Proc. Combust. Inst. 33 (2011) 1113–1120.

[15] I. Chterev, C.W. Foley, D. Foti, S. Kostka, A.W. Caswell, N. Jiang, A. Lynch, D.R. Noble, S. Menon, J.M. Seitzman, T.C. Lieuwen, Flame and flow topologies in an annular swirling flow, Combust. Sci. Technol. 186 (8) (2014) 1041–1074.

[16] T. Lu, C.K. Law, A criterion based on computational singular perturbation for the identification of quasi steady state species: a reduced mechanism for methane oxidation with NO chemistry, Combust. Flame 154 (4) (2008) 761–774.

[17] R. Price, I. Hurle, T. Sudgen, Optical studies of the generation of noise in turbulent flames, Symp. (Int.) Combust. 12 (1968) 1093–1102.

[18] T. Schuller, D. Durox, S. Candel, Dynamics of and noise radiated by a perturbed impinging premixed jet flame, Combust. Flame 128 (2002) 88–110.

[19] J. Li, D. Durox, F. Richecoeur, T. Schuller, Analysis of chemiluminescence , density and heat release rate fluctuations in acoustically perturbed laminar premixed flames, Combust. Flame 162 (2015) 3934–3945.

[20] D. Durox, T. Schuller, N. Noiray, S. Candel, Experimental analysis of nonlinear flame transfer functions for different flame geometries, Proc. Combust. Inst. 32 (1) (2009) 1391–1398.

[21] A. Birbaud, D. Durox, S. Ducruix, S. Candel, Dynamics of confined premixed flames submitted to upstream acoustic modulations, Proc. Combust. Inst. 31 (2007) 1257–1265.

[22] O. Colin, M. Rudgyard, Development of high-order Taylor–Galerkin schemes for LES, J. Comput. Phys. 162 (2) (2000) 338–371.

[23] V. Moureau, G. Lartigue, Y. Sommerer, C. Angelberger, O. Colin, T. Poinsot, Numerical methods for unsteady compressible multi-component reacting flows on fixed and moving grids, J. Comput. Phys. 202 (2) (2005) 710–736.

[24] T. Poinsot, S. Lele, Boundary conditions for direct simulations of compressible viscous flows, J. Comput. Phys. 101 (1) (1992) 104–129.

[25] J.O. Hirschfelder, C.F. Curtiss, R.B. Bird, Molecular theory of gases and liquids, John Wiley, 1954.

[26] M. Miguel-Brebion, Joint numerical and experimental study of thermo-acoustic instabilities, Institut National Polytechnique de Toulouse, 2017 Ph.D. thesis.

[27] V.A.L. Erie, V. Frayssé, L. Giraud, S. Gratton, A set of GMRES routines for real and complex arithmetics on high performance computers, ACM Trans. Math. Softw. (TOMS) 31 (2) (2005) 228–238.

[28] J. Donea, A. Huerta, Finite element methods for flow problems, John Wiley & Sons, 2003.

[29] S. Buis, A. Piacentini, D. Déclat, The PALM Group, PALM: a computational framework for assembling high-performance computing applications, Concurr. Comput. 18 (May 2004) (2006) 231–245.

[30] S. Berger, S. Richard, F. Duchaine, G. Staffelbach, L.Y.M. Gicquel, On the sensitivity of a helicopter combustor wall temperature to convective and radiative thermal loads, Appl. Thermal Eng. 103 (2016) 1450–1459.

[31] M.-P. Errera, F. Duchaine, Comparative study of coupling coefficients in Dirichlet Robin procedure for fluid–structure aero thermal simulations, J. Comput. Phys. 312 (2016) 218–234.

[32] M. Boileau, F. Duchaine, J.C. Jouhaud, Y. Sommerer, Large-eddy simulation of heat transfer around a square cylinder using unstructured grids, AIAA J. 51 (2) (2013) 372–385.

[33] T. Schuller, D. Durox, S. Candel, A unified model for the prediction of laminar flame transfer functions, Combust. Flame 134 (1–2) (2003) 21–34.

[34] T. Lieuwen, Modeling premixed combustion acoustic wave interactions: a review, J. Propuls. Power 19 (5) (2003) 765–781.

[35] R. Rook, L. de. Goey, L. Somers, K. Schreel, R. Parchen, Response of burner-stabilized flat flames to acoustic perturbations, Combust. Theory Modell. 6 (2) (2002) 223–242.

[36] A. Cuquel, D. Durox, T. Schuller, Impact of flame base dynamics on the nonlinear frequency response of conical flames, Comptes Rendus Mécanique 341 (2013) 171–180.

[37] V. Kornilov, R. Rook, J. ten Thije Boonkkamp, L. de Goey, Experimental and numerical investigation of the acoustic response of multi-slit bunsen burners, Combust. Flame 156 (10) (2009) 1957–1970.

[38] D. Mejia, Wall-temperature effects on flame response to acoustic oscillations, Université de Toulouse, 2014 Ph.D. thesis.

[39] F. Boudy, D. Durox, T. Schuller, S. Candel, Nonlinear mode triggering in a multiple flame combustor, Proc. Combust. Inst. 33 (2011) 1121–1128.

[40] W. Polifke, A. Gentemann, Order and realisability of impulse response filters for accurate identification of acoustical multi-ports from transient CFD, J. Sound Vib. 9 (3) (2004) 139–148.

[41] F. Duchaine, F. Boudy, D. Durox, T. Poinsot, Sensitivity analysis of transfer functions of laminar flames, Combust. Flame 158 (12) (2011) 2384–2394.

[42] K. Truffin, T. Poinsot, Comparison and extension of methods for acoustic identification of burners, Combust. Flame 142 (4) (2005) 388–400.

[43] N. Noiray, D. Durox, T. Schuller, S. Candel, A unified framework for nonlinear combustion instability analysis based on the flame describing function, J. Fluid Mech.. 615 (2008) 139–167.

[44] S. Candel, D. Durox, T. Schuller, J.-F. Bourgouin, J.P. Moeck, Dynamics of Swirling Flames, Ann. Rev. Fluid Mech. 46 (1) (2014) 147–173.

[45] J.-F. Bourgouin, D. Durox, J.P. Moeck, T. Schuller, S. Candel, Characterization and modeling of a spinning thermoacoustic instability in an annular combustor equipped with multiple matrix injectors, J. Eng. Gas Turb. Power 137 (2) (2015) 021503.

[46] S. Föller, W. Polifke, Identification of aero-acoustic scattering matrices from large eddy simulation. Application to a sudden area expansion of a duct, J. Sound Vib. 331 (13) (2012) 3096–3113.

[47] L. Chong, T. Komarek, R. Kaess, S. Foller, W. Polifke, Identification of flame transfer functions from les of a premixed swirl burner, in: A. P. (Ed.), ASME Turbo Expo, Glasgow, UK, 2010. [GT2010-22769] http://proceedings.asmedigitalcollection.asme.org/proceeding.aspx?articleid=1608188

[48] W. Polifke, Black-box system identification for reduced order model construction, Ann. Nuclear Energy 67 (2014) 109–128.

[49] M. Fleifil, A. Annaswamy, Z. Ghoneim, A. Ghoniem, Response of a laminar premixed flame to flow oscillations: a kinematic model and thermoacoustic instability results, Combust. Flame 106 (4) (1996) 487–510.

[50] A.-L. Birbaud, D. Durox, S. Candel, Upstream flow dynamics of a laminar premixed conical flame submitted to acoustic modulations, Combust. Flame 146 (3) (2006) 541–552.